The influence of stereochemistry on the reactivity of the Diels–Alder cycloaddition and the implications for reversible network polymerization

Cuvellier, Audrey; Verhelle, Robrecht René; Brancart, Joost; Vanderborght, Bram; Van Assche, Guy; Rahier, Hubert

Published in:
Polymer Chemistry

DOI:
10.1039/c8py01216d

Publication date:
2019

ARTICLE Journal Name

The influence of stereochemistry on the reactivity of the Diels-Alder cycloaddition and the implications for reversible network polymerization.

Received 00th January 20xx,
Accepted 00th January 20xx

DOI: 10.1039/x0xx00000x

www.rsc.org/

Audrey Cuvellier,[a] Robrecht Verhelle,[a] Joost Brancart,[a,b] Bram Vanderborght,[b] Guy Van Assche *[a] and Hubert Rahier [a]

A detailed calorimetric investigation is performed on the influence of the stereochemistry of the furan-maleimide Diels-Alder reaction on the kinetics of the reversible network formation, in the absence of solvents. Two stereoisomers are formed, with the endo isomer forming kinetically faster and undergoing cycloreversion at lower temperatures than the more thermodynamically stable exo isomer. Rate constants and activation energies for the forward and retro Dials-Alder reaction of both stereoisomers were derived by modelling isothermal (microcalorimetry) and non-isothermal (DSC) data. The kinetic model was further verified using time-resolved and temperature-controlled ^{1}H NMR spectroscopy. The influence of time, temperature, and the maleimide/furan ratio on the exo/endo ratio are presented. The implications of the formation of two stereoisomers on the thermoresponsiveness and thermal behaviour for thermal processing and self-healing applications are discussed.

Introduction

The Diels-Alder reaction, first described by Otto Diels and Kurt Alder, is one of the most studied thermoreversible equilibrium reactions[1]. This [4+2] cycloaddition reaction between a conjugated diene and a dienophile results in the formation of a Diels-Alder cycloadduct. The equilibrium is such that at low temperatures the Diels-Alder cycloadduct is formed predominantly, whereas at higher temperatures the equilibrium shifts towards the reactants. At every temperature a dynamic equilibrium exists between the forward Diels-Alder reaction and the backward retro-Diels-Alder reaction. The most studied Diels-Alder reaction is the cycloaddition of furan (diene) and maleimide (dienophile). Their fast reaction kinetics and high conversion at ambient temperature make them suitable candidates for thermoresponsive materials, such as, thermoremendable and self-healing polymer networks, which can be reshaped and healed at mildly elevated temperatures (80°C – 140°C) due to the thermoreversible crosslinking [2–5]. In previous work, these materials have been employed in self-healing coatings [4–6] and self-healing soft robotic actuators [7–9]. In this work, the reaction kinetics of the Diels-Alder reaction between furan and maleimide is thoroughly investigated in view of their processing, manufacturing and aforementioned applications.

Depending on the suprafacial approach between the furan and maleimide functional groups, two stereoisomeric cycloadducts can be formed (Figure 1a). The endo isomer, where the bulkier sides of the diene and dienophile overlap, is formed faster due to secondary interactions between the bulkier sides resulting in a lower activation energy barrier. The exo isomer, formed when the bulkier sides of the diene and dieneophile lie away from each other, is the more thermodynamically stable adduct (more negative free energy of reaction) since less steric hindrance is present than for the endo isomer (Figure 1b)[10]. Although the stereochemistry is well documented in literature[11,12], its effect on the reactivity and the thermoreversibility is often overlooked in discussions of the thermoreversible network formation. Most of the kinetic studies have been performed using Infrared spectroscopy [6,13–15], however, this technique does not allow to differentiate between the endo and exo forms [14], so the isomers are lumped together in the kinetic analysis. The few kinetic studies[16–18] determining kinetic parameters for both isomers separately were performed in a solvent, affecting the reaction kinetics, as shown in [14], where different kinetic parameters are obtained for the same reaction performed in chloroform and acetonitrile. In this work, an amorphous, liquid bismaleimide is used in combination with an amorphous, liquid furan-functionalized poly (propylene oxide), allowing the kinetic evaluation of the bulk reactive system, without the interference of a solvent. Microcalorimetry (TAM) and differential scanning calorimetry (DSC) are used to study the reaction and for deriving the kinetic parameters of the 2-equilibrium reaction model. Microcalorimetry will be used to follow the formation of the Diels-Alder adducts starting from a liquid mixture of reagents, while the DSC measurements will be used to follow the decomposition process of the adducts upon heating mixtures previously reacted under well-chosen conditions. The model is confirmed by ^{1}H NMR spectroscopy measurements.

Commented [a1]: Marked in yellow what has been added to the text, marked in blue what has been moved from the results and discussion section to the experimental section

[a] *Physical Chemistry and Polymer Science (FYSC), Vrije Universiteit Brussel (VUB), Pleinlaan 2, B-1050 Brussels, Belgium*
[b] *Robotics and Multibody Mechanics (R&MM) and Flanders Make, Vrije Universiteit Brussel (VUB), Pleinlaan 2, B-1050 Brussels, Belgium*
* Guy.Van.Assche@vub.be
Electronic Supplementary Information (ESI) available: [details of any supplementary information available should be included here]. See DOI: 10.1039/x0xx00000x

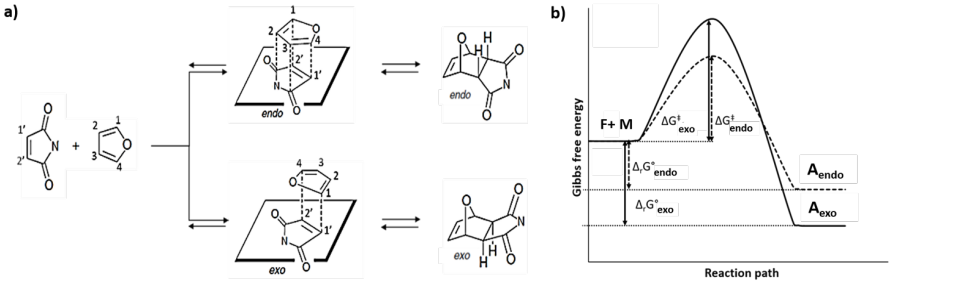

Figure 1: a) Stereochemistry of the furan-maleimide reaction resulting in an endo and an exo isomer. b) The Gibbs free energy profiles with the activation energy barriers $\Delta G^{\ddagger}$ and the (standard) Gibbs free energies of reaction $\Delta_r G^{\circ}$ for furan and maleimide that forms two products, the exo isomer, which has a higher activation energy barrier and a higher Gibbs free energy of reaction than the endo isomer.

Experimental

Materials

A Jeffamine D400, poly (propylene oxide) bis(2-amino propyl ether) (J400) with repeated oxypropylene units in the backbone and an average molecular weight of 430 $g.mol^{-1}$, was supplied by Huntsman (Belgium). Furfuryl glycicyl ether (FGE) was purchased from Sigma Aldrich. A poly (propylene oxide) 400 bismaleimide (M400) derived from Jeffamine D400 was purchased from Specific Polymers. The monomers are shown in Chart 1 and were used as purchased. FGE and M400 are stored in refrigerated conditions. M400 is stored under nitrogen. Poly(propylene glycol) with an average molecular weight of about 425 g mol^{-1} (PPG 425) was purchased from Sigma Aldrich.

Synthesis of the Diels-alder epoxy-amine networks

The furan and maleimide functionalized epoxy-amine polymer networks were synthesized using a two-step procedure. First, a tetrafunctional furan compound (F400) was formed by the irreversible epoxy-amine reaction between the tetrafunctional Jeffamine D400 and a stoichiometric amount of the monofunctional furfuryl glycidyl ether. This reaction is performed without the use of any solvent or catalyst, for 7 days at 60°C followed by 2 days at 90°C to ensure a functionality of at least 3.8 for the furan-functionalized Jeffamine (functionalization > 95 %)[4–6]. In a second step, this furan-functionalized compound F400 is reversibly crosslinked with the bifunctional maleimide M400 to form a reversible Diels-Alder epoxy-amine network. The F400 and M400 compounds are both liquid at ambient temperature and highly compatible and can thus be mixed without the need for a solvent. Fresh, unreacted mixtures were used for the kinetic evaluation.

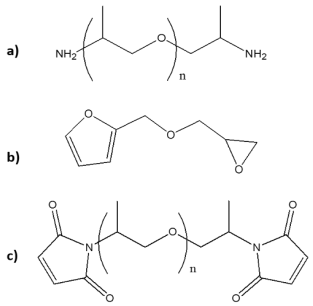

Chart 1: Monomers used for the synthesis of the reversible network: a) J400, b) FGE and c) M400 with n=6.1 for J400 and M400.

Techniques

A TA Instruments Thermal Activity Monitor III (TAM), a microcalorimeter equipped with two multicalorimeter units containing six 4-mL minicalorimeters each, was used to study the isothermal reaction of freshly prepared mixtures in 4-mL crimp seal glass ampoules. The temperature in the lab and the time needed between adding the components together and introducing the sample in the TAM were measured and taken into account for the evaluation of the experimental data. Before introducing the samples into the measuring position of the minicalorimeter, the samples remain 15 minutes in an equilibration position. The thermostat temperature accuracy of ± 0.1 K and temperature stability of ± 100 µK over the course of 24 h result in a heat flow signal noise of ± 200 nW and a baseline drift of less than 250 nW over the course of 24 h. Isothermal TAM measurements following the formation of the adducts starting from freshly mixed reagents were performed at different isothermal temperatures and for different maleimide/furan ratios *r.* Given that the instrument baseline varies less than ±250 nW, at least a factor 17 smaller than the smallest heat flow measured at the end of the TAM experiment, the measured heat flow can be considered as the absolute heat flow due to the reaction and thus no further data treatment is required.

Differential scanning calorimetry (DSC) was performed using a TA instruments Discovery DSC. The DSC was equipped with a refrigerated cooling system (RCS) that allows cooling down to -90°C. Nitrogen was used as purge gas and the samples were

measured in Tzero pans with perforated Tzero hermetic lids to ensure an inert atmosphere above the sample. The freshly mixed samples were stored in liquid nitrogen to avoid reaction during storage. The following temperature program was used with various (T_{iso}, t_{iso}) combinations:

$$(25°C, 1\ min) \xrightarrow{5\ K.min^{-1}} (T_{iso}, t_{iso}) \xrightarrow{20\ K.min^{-1}} (-90°C, 5\ min) \xrightarrow{5\ K.min^{-1}} 200°C$$

For the DSC measurements, only the experimental data obtained during the second heating step was used to model the reactions. The DSC thermograms of the second heating in Figure 2 show a glass transition followed by a combination of endothermic and exothermic peaks arising from the reactions. Consequently, several data treatment steps are needed before the reaction exotherms and endotherms can be modelled.
The heat flow measured in DSC is generally represented by (equation 1)[21].

$$q = C_p \frac{dT}{dt} + f(T(t), t) + \text{instrument}(T(t)) \quad (1)$$

Where q (in W.g^{-1}) is the heat flow signal normalized against the sample weight, C_p is the specific heat capacity of the sample, $f(T(t),t)$ represents the heat flow resulting from kinetic events (the reactions in the present study), and $instrument(T(t))$ represents the contribution of the instrument, which can be measured using empty sample and reference pans. For the measurements performed, the instrument contribution of the Discovery DSC proved negligible compared to the reaction heat flows. To subtract the heat capacity contribution, the straight section between the glass transition and the first exothermic or endothermic peak was used to fit the baseline (fitted individually for each measurement). An example of a fitted baseline is shown in Figure 2a, while the reaction heat flows obtained after subtraction are given in Figure 2b. After baseline subtraction, the only contribution to the $f(T(t),t)$ term is the heat of reaction, permitting modelling of the heat flow signals originating from the reactions only.

To confirm the obtained model, time-resolved and temperature-controlled liquid state ^{1}H NMR spectroscopy (Bruker Avance 250 MHz) was used to quantitatively follow the concentrations of furan, maleimide, endo adduct, and exo adduct as a function of time during isothermal reaction at 56.6°C. The measurements were made starting with a freshly prepared mixture of M400, FGE and PPG 425. The F400 was replaced by FGE and PPG 425 to retain sufficient mobility by avoiding network formation yet maintaining the same concentration of maleimide and furan as for the F400-M400 system. As an external lock signal, a capillary with toluene-D8 containing 0.03 v% TMS was inserted in the NMR tube containing the freshly prepared mixture. The temperature in the NMR spectrometer was determined from the difference in chemical shift $\Delta\delta$ between the CH_2 and OH peaks of ethylene glycol using equation (2)[19].

$$T(\mathrm{K}) = 466.5 - 102.00\ \Delta\delta \quad (2)$$

To monitor the concentrations over a period of two days, a spectrum was taken every 2 minutes the first hour, every 6 minutes the second hour, every 15 minutes for the following 13 h, and every hour for the next 33 h. For each measurement 8 acquisitions were taken with in-between each scan a relaxation delay of 10 seconds to give the aromatic protons sufficient time to relax.

Kinetic simulations

For modelling the reaction kinetics, a mechanistic model is used that considers the equilibrium reactions between furan F, maleimide M, and the stereoisomeric adducts A_{endo} and A_{exo}:

$$\mathrm{A_{endo}} \underset{k_{\mathrm{rDA,endo}}}{\overset{k_{\mathrm{DA,endo}}}{\leftrightharpoons}} \mathrm{F + M} \underset{k_{\mathrm{rDA,exo}}}{\overset{k_{\mathrm{DA,exo}}}{\rightleftharpoons}} \mathrm{A_{exo}}$$

All reactions are elementary reaction steps. The direct isomerization from endo to exo adduct was not accounted for, as it needs to be preceded by the cycloreversion of the endo adduct into its monomers, as previously stated by Froidevaux *et al.* [18]. The kinetics of the Diels-Alder and retro Diels-Alder reactions are described for both stereoisomers by their corresponding rate constants ($k_{DA,endo}$, $k_{rDA,endo}$, $k_{DA,exo}$, and $k_{rDA,exo}$).

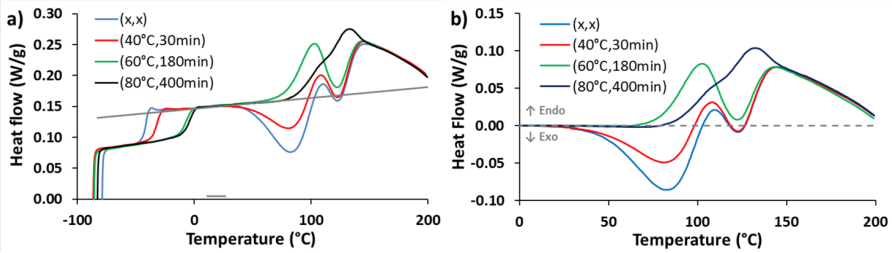

Figure 2: Overlay of DSC thermograms (exo down) of the heating step after the (T_{iso}, t_{iso}) temperature treatment for a F400-M400 (r=1) system: a) the curves as obtained showing a glass transition temperature and several exothermic and/or endothermic peaks, with an example of a fitted baseline and the temperature interval over which was fitted indicated at the bottom of the figure and b) after subtraction of the glass transition step and baseline.

The mechanistic model corresponds to a set of ordinary differential equations (ODE) describing the variation of the concentrations of all components (Equation (3)).

$$\frac{\mathrm{d}[\mathrm{C}_i]}{\mathrm{d}t} = \sum_{j}^{N} v_j \quad (3)$$

with $[\mathrm{C_i}]$ (mol.kg^{-1}) the concentration of component *i*, $\mathrm{d}[\mathrm{C_i}]/dt$ (mol.kg^{-1}.s^{-1}) the production rate of component *i*, *N* the number of reactions, v_j (mol.kg^{-1}.s^{-1}) the formation (or consumption) rate of component *i* in reaction *j*, which depends on the concentrations of the reagents involved and the rate constant of the reaction. The differential equations can be related to the measured reaction heat flow curves through Equation (4).

$$f(T(t), t) = q_r = \sum_{j}^{N} \frac{d[C_i]}{dt} \Delta_f H_i^0 \quad (4)$$

with q_r (in W.g^{-1}) the heat flow signal normalized against the sample weight and $\Delta_f H_i^0$ (kJ.mol^{-1}) the enthalpy of formation of component *i*.

For the modelling, an in-house developed Matlab software was used. For the numerical integration of the ODE, ODE15s was used. To fit the calculated heat flow curves to the experimental isothermal (TAM) and non-isothermal (DSC) data, the logarithm of the four rate constants at a reference temperature of 25 °C and their activation energies ($E_{\mathrm{DA,endo}}$, $E_{\mathrm{rDA,endo}}$, $E_{\mathrm{DA,exo}}$, $E_{\mathrm{rDA,exo}}$) were optimized. The natural logarithm of the pre-exponential factors ($\ln(A_{\mathrm{DA,endo}})$, $\ln(A_{\mathrm{rDA,endo}})$, $\ln(A_{\mathrm{DA,exo}})$, $\ln(A_{\mathrm{rDA,exo}})$) was determined from the optimized rate constant and activation energies. For the least square optimization of the kinetic parameters in the reaction model, a sum of weighted squares of the differences between the experimental and modelled data was minimized. For the TAM measurements, a weight factor of 10 was given to data points at the start of the experiment (up to 70% conversion), a factor of 5 up to 90% conversion, and a weight of 1 to the tail of the experiment. If an equal weight was given to all points, the tail, which contains much more points than the reaction peak, would have a larger impact on the optimisation of the sum of squares. The DSC experiments were only fitted until a cut-off temperature of 130 °C by giving all points up to 130 °C a weight of one, and those above a zero weight, eliminating data at elevated temperatures where potentially side reactions, such as Michael addition reactions [22] and homopolymerization of the maleimide [6], take place.

The optimized kinetic parameters were used to determine the thermodynamic parameters for both isomers using equation 5-8, with 'i' indicating the endo or exo adduct, $\Delta_r G^0_i$, $\Delta_r H^0_i$ and $\Delta_r S^0_i$ the standard reaction Gibbs energy, enthalpy, and entropy, respectively and C_0 a standard concentration of 1 mol.kg^{-1}.

$$\Delta_r G^0{}_i = -RT\ln K_{P,i} \quad (5)$$

$$K_{C,i} = \frac{k_{\mathrm{DA},i}\, C_0}{k_{\mathrm{rDA},i}} \quad (6)$$

$$k_{\mathrm{DA},i} = A_{\mathrm{DA},i}\, e^{\frac{-E_{\mathrm{DA},i}}{RT}} \quad , \quad k_{\mathrm{rDA},i} = A_{\mathrm{rDA},i}\, e^{\frac{-E_{\mathrm{rDA},i}}{RT}} \quad (7)$$

$$\Delta_r G^0{}_i = \Delta_r H^0{}_i - \mathrm{T}\Delta_r S^0{}_i \quad (8)$$

Results and discussion

Experimental approach

The influence of stereochemistry on the reactivity of a tetrafunctional furan compound (F400) and a bifunctional maleimide (M400) was studied using isothermal TAM and non-isothermal DSC experiments, summarized in Table 1. In a previous study, isothermal microcalorimetry experiments were performed and interpreted using a single equilibrium reaction, not differentiating between the two stereoisomers[20]. In this work, modelling only isothermal measurements at relatively low temperatures proved to insufficiently discriminate between the formation of one or two adducts: both models fit the isothermal microcalorimetry results well. To unravel the reaction kinetics of the two stereoisomers, it proved crucial to model the exothermic and endothermic peaks observed in non-isothermal DSC measurements (e.g., Figure 2), in addition to isothermal microcalorimetry measurements.

The temperature programs of the DSC experiments (Table 1) were carefully chosen to enhance the reliability of the kinetic modelling. By treating the reaction mixtures for different isothermal times and temperatures (T_{iso},t_{iso}), very different heat flow profiles were observed in the consecutive heating

Table 1: Isothermal TAM and non-isothermal DSC experiments for various maleimide/furan ratios (r) using different heat treatments.

Technique	r	Experiments
TAM*	1	T_{iso}= 15°C, 25°C, 40°C
	0.7	T_{iso}= 25°C, 40°C
	2	T_{iso}= 25°C, 40°C
DSC°	1	(T_{iso},t_{iso})= (x,x), (40°C,30 min), (60°C,20 min,180 min,420 min, 900 min), (80°C, 400 min)
	0.7	(T_{iso},$t_{\mathrm{iso's}}$)= (40°C, 30 min,180 min), (60°C,30 min,180 min, 420 min), (80°C, 30 min, 180 min,400 min)
	2	(T_{iso},t_{iso})= (40°C,30 min,180 min), (60°C,30 min,180 min, 420 min,900min), (80°C, 30 min,400 min)

* For TAM the isothermal temperature at which the experiment was performed is given.

° for DSC the (T_{iso},$t_{\mathrm{iso's}}$) temperature treatments show how the t_{iso} was varied for the same T_{iso}. (x,x) is when there is no isothermal treatment and thus the sample is immediately cooled to -90°C and heated to 200°C.

step (Figure 2), indicating that quite different concentrations (and ratios) of the exo and endo isomers were obtained after the isothermal treatment. In case of shorter isothermal

treatments at lower temperatures, e.g., 30 min at 40°C, also large exothermic peaks are seen, as well as a small exothermic peak in between the two endothermic contributions. These observations indicate that the reaction upon heating is certainly more complex than just the consecutive decomposition of the endo and the exo isomer.

By careful design of the DSC experiments used for the modelling, the reaction model is forced to fit the experimental data for both exothermic and endothermic (overall) heat flows, and thus for both bond-forming and bond-breaking reactions, making the model much more robust than in case of using isothermal (overall bond-forming) data only. The selection of the experimental conditions (T_{iso},t_{iso}), was further supported by performing simulations with kinetic models optimized on more limited experimental data sets, looking for extreme cases and distinguishing features (like the small exotherm in between the two endotherms). Additional experiments were performed to be able to model the influence of t_{iso} for the same T_{iso}, and the influence of T_{iso} for the same t_{iso}. The effect of changing the maleimide/furan ratio was also studied to have a better determination of the kinetic constants, step by step leading to a more accurate model.

Modelling results

The optimized kinetic model involving the two stereoisomers fits the extensive data set very well. For the DSC experiments, the largest difference between the experimental and modelled data was 0.007 W g^{-1} corresponding to a relative error of 8 %. For TAM, the difference in the integration of the reaction exotherm of the experimental and modelled data varies between 1 and 8 J g^{-1} corresponding to a relative error between 2 % and 13 %.

By modelling the reaction data obtained from TAM and DSC experiments, the optimized kinetic parameters were obtained, and from these, the reaction enthalpies and entropies were derived (Table 2). The kinetic parameters previously obtained while considering only one equilibrium[20], not distinguishing between exo and endo isomers, correspond fairly well to the new kinetic parameters obtained for the endo isomer. This can be understood by realizing that the old data only involved the (overall) formation of adducts for isothermal measurements in a limited low temperature interval only (25 °C to 90 °C), conditions in which the endo isomer is most important. The new kinetic data take into account the formation and dissociation of the two adducts in a much larger temperature interval (0°C to 130 °C).

Influence of t_{iso} for the same T_{iso}

Figure 3a shows the influence of changing the isothermal reaction time (t_{iso}: 20, 180, 420, 900 min), at a constant temperature of 60 °C and for a stoichiometric maleimide/furan ratio, on the heat flow profiles of the subsequent heating. After 20 min at 60 °C, upon heating from -90°C, an exothermic peak is seen, followed by two endothermic peaks. The exothermic peak corresponds to the formation of the Diels-Alder adducts (Figure 3c). When no or only a short isothermal treatment is given at 60°C (or lower), there is still a significant fraction of unreacted maleimide and furan that will react during the heating step following the isothermal treatment. This can also be seen in Figure 3b, showing the concentrations of endo (dash double dotted lines) and exo (solid lines) adducts as a function of temperature. Except for the shortest time (20 min), the concentrations for the endo and exo adducts stay constant below 80 °C. For the blue lines corresponding to (60 °C, 20 min), an increase in concentration is seen for both adducts below 80 °C. At the start of the heating, the sum of the concentrations of both isomers is 1.4 mol.kg^{-1} for t_{iso} equal to 180, 420 and 900 min, while being less than 1.0 mol.kg^{-1} for 20 min, proving that less Diels-Alder adduct was formed during the isothermal segment, thus inducing the formation of adduct during the subsequent heating. For t_{iso} equal to 180, 420 and 900 min only the two endothermic peaks are seen in the experimental heat flow (Figure 3a). The longer the isothermal times, the smaller the first endothermic peak, the bigger the second endothermic peak, and especially, the less deep the valley in between them. As shown in Figure 3c-e, the first endothermic peak corresponds to the combined contribution of the endothermic cycloreversion of the endo adduct and the exothermic formation of the exo adduct, the latter being due to the increased maleimide and furan concentrations originating from the cycloreversion of the endo adduct. The longer the isothermal treatment, the larger concentration of exo adduct (Figure 3b) present after the longer isothermal treatment, and the smaller the exothermic contribution due to the formation of additional exo adduct. For t_{iso} = 900 min (Figure 3f), the first endothermic peak corresponds to the cycloreversion of the endo isomer only, as no more additional exo isomer is formed. In all cases the second endothermic peak is due to the retro Diels-Alder reaction of the exo adduct [18,23]. The cycloreversion of the exo adduct occurs at higher temperatures than for the endo adduct due to a higher activation energy barrier for the

Table 2: Kinetic and thermodynamic parameters obtained for the F400-M400 system with our model and compared to the parameters obtained when considering only one isomer.

Kinetic / thermodynamic parameters	F400-M400 Two isomers	F400-M400 [20] Endo isomer
$\ln(A_{DA,endo})$ (kg.mol^{-1}.s^{-1})	13.1	11.7
$E_{DA,endo}$ (kJ.mol^{-1})	58.5	53.9
$\ln(A_{rDA,endo})$ (s^{-1})	31.0	28.3
$E_{rDA,endo}$ (kJ.mol^{-1})	113.0	105.7
$\ln(A_{DA,exo})$ (kg.mol^{-1}.s^{-1})	13.6	X
$E_{DA,exo}$ (kJ.mol^{-1})	62.6	X
$\ln(A_{rDA,exo})$ (s^{-1})	31.5	X
$E_{rDA,exo}$ (kJ.mol^{-1})	122.6	X
$\Delta_r H^0_{endo}$ (kJ.mol^{-1})	-54.6	-51.8
$\Delta_r S^0_{endo}$ (J.mol^{-1}.K^{-1})	-149.1	-138.0
$\Delta_r H^0_{exo}$ (kJ.mol^{-1})	-60.0	X
$\Delta_r S^0_{exo}$ (J.mol^{-1}.K^{-1})	-149.5	X

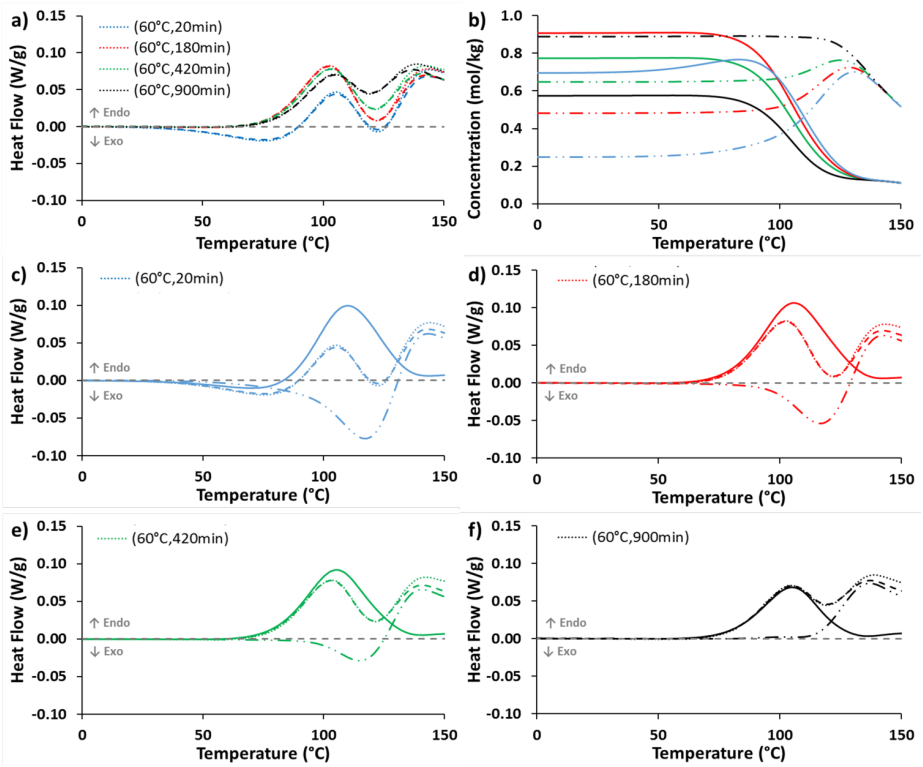

Figure 4: a) Overlay of the experimental (dotted line) and modelled (dashed line) reaction heat flow profiles (exo down) for the heating after (60°C, 20 min), (60°C, 180 min), (60°C, 420 min) and (60°C, 900 min) for a F400-M400 (r=1) system. b) the corresponding concentration profiles of the endo adduct (solid line) and exo adduct (dash double dot line). The reaction heat flow due to the endo adduct (solid line) and exo adduct (dash double dot line) is overlaid with the experimental and modelled heat flow for c) (60°C,20min), d) (60°C,180min), e) (60°C,420min) and f) (60°C,900min).

retro Diels-Alder reaction of the exo adduct (Table 2). The faster formation of the kinetically favoured endo adduct, which can be concluded from $E_{DA,endo} < E_{DA,exo}$ in Table 2 and from a higher rate constant $k_{DA,endo}$ in Table 3, can be most easily observed in the simulated concentration profiles for the isothermal treatment at 60°C (Figure 4). At first, the endo isomer is formed much faster than the exo isomer, but with increasing isothermal reaction time, the

Table 3: Kinetics and thermodynamic results for F400-M400 at 25°C and 60°C.

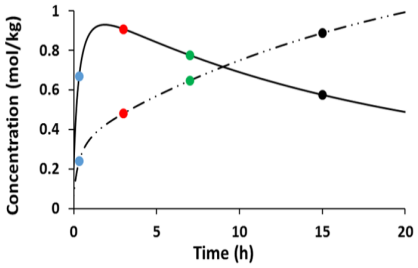

Figure 3: Concentration profiles of the endo (solid line) and exo adduct (dash double dot line) as a function of time at T_{iso} 60°C for a F400-M400 (r=1) system. The concentrations of (60°C, 20 min) (blue), (60°C, 180 min) (red), (60°C, 420 min) (green) and (60°C,900 min) (black) after their isothermal segments were added on the graph.

Kinetic / thermodynamic results	25°C	60°C
$\ln(k_{DA,endo})$ (kg.mol^{-1}.s^{-1})	-10.5	-8.0
$\ln(k_{rDA,endo})$ (s^{-1})	-14.6	-9.8
$\ln(k_{DA,exo})$ (kg.mol^{-1}.s^{-1})	-11.7	-9.1
$\ln(k_{rDA,exo})$ (s^{-1})	-17.9	-12.7
$\Delta_r G^0_{endo}$ (kJ.mol^{-1})	-10.1	-4.9
$\Delta_r G^0_{exo}$ (kJ.mol^{-1})	-15.4	-10.2
K_{endo}	59.5	5.9
K_{exo}	503.9	39.6

during reaction at 56.6 °C inside the NMR spectrometer. Figure 5a shows the evolution of the aromatic resonance peaks as a function of time. The overlay over the entire spectral width was added in supplementary information. Several peaks can be seen in the aromatic region[18,23]: 1 H from furan at 7.3 ppm, 2 H's from maleimide at 6.6 ppm, 2 H's from the exo adduct at 6.4 ppm, and 4 H's (2 H's +2 H's) from furan and the endo adduct at 6.2 ppm. A decrease in intensity is seen as a function of time for the furan and maleimide peaks at 7.3 and 6.6 ppm, respectively, as

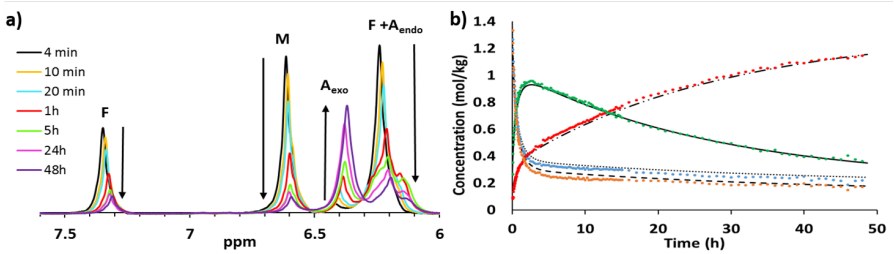

Figure 5: ^{1}H NMR results for the reaction of a FGE-M400-PPG425 mixture with r=0.96 at 56.6°C over a period of 48 h. a) Overlay of ^{1}H NMR spectra, zoomed in on the aromatic region, showing the evolution of resonance peaks due to furan, maleimide and both adducts in time. b) Overlay of the modelled and ^{1}H NMR concentration profiles. The modelled concentrations are shown in black: furan (dotted line), maleimide (dashed line), endo adduct (solid line) and the exo adduct (dash double dot line). The experimental data are shown using coloured dots: furan (blue), maleimide (orange), endo adduct (green), and exo adduct (red).

endo isomer concentration starts decreasing, while the exo isomer concentration increases monotonously, shifting the balance towards the more thermodynamically stable exo isomer. This explains why the second endothermic peak (Figure 3a) becomes larger with increasing isothermal time. After 9 hours, the endo and exo adduct concentrations are equal and for longer times the exo adduct becomes the larger fraction. The higher thermodynamic stability of the exo isomer at 60°C is also seen as a more negative reaction Gibbs free energy (Table 3).

Confirmation of the model through ^{1}H NMR

As the calorimetric data do not give direct proof of the exo and endo adduct concentrations, the model was confirmed using time-resolved ^{1}HNMR spectroscopy. The concentration of maleimide, furan, endo adduct, and exo adduct were followed well as for the merged furan and endo adduct peak at 6.2 ppm, while the peak corresponding to the exo adduct at 6.4 ppm grows in intensity. The entire NMR spectrum and peak association can be found in supplementary information.

The normalized peak integrations in the aromatic region were used to determine the concentrations of furan, maleimide, endo adduct, and exo adduct. The concentration of the endo adduct is determined by subtracting the concentration of furan from the concentration corresponding to the combined furan and endo adduct peak. This was done for all spectra individually, leading to concentration profiles for furan, maleimide, endo adduct and exo adduct. An overlay of these concentration profiles and the concentration profiles calculated using the 2-equilibrium model with the optimized kinetic parameters (Table 2) and the starting furan and maleimide concentrations are

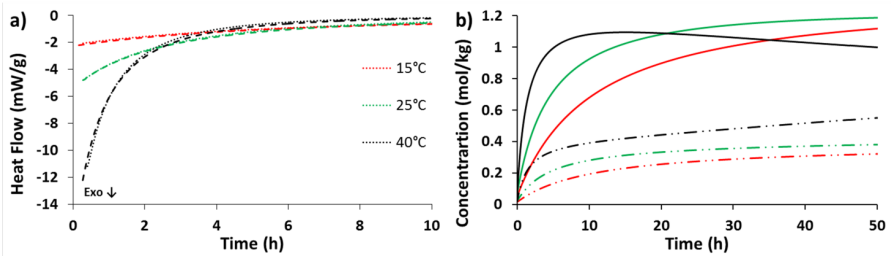

Figure 6: a) Overlay of the experimental (dotted line) and modelled (dashed line) microcalorimetry heat flow profiles (exo down) for T_{iso}= 15 °C, 25 °C and 40 °C for a F400-M400 (r=1) system. b) the corresponding concentration of the endo adduct (solid line) and exo adduct (dash double dot line).

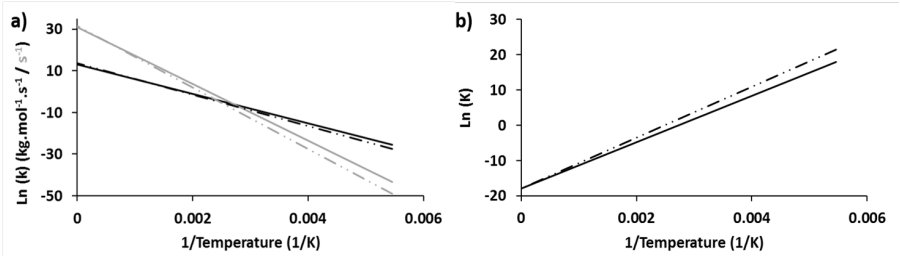

Figure 7: a) Logarithm of the rate constants as a function of the inverse temperature with Diels-Alder constants in black and the retro Diels-Alder constants in grey. b) The equilibrium constants as a function of the inverse temperature. The endo constants are indicated with a solid line, the exo constants with a dash double dot line.

shown in Figure 5b. A very good correspondence is seen between the experimentally determined and modelled curves, confirming the reliability of the model and the related kinetic parameters obtained using data from isothermal and non-isothermal calorimetric experiments only.

Influence of T_{iso}

The influence of the reaction temperature (15 °C, 25 °C and 40 °C) on isothermal (microcalorimetry) measurements starting from fresh stoichiometric F400-M400 mixtures is shown in Figure 6. In Figure 6a, the heat flow is the most exothermal at

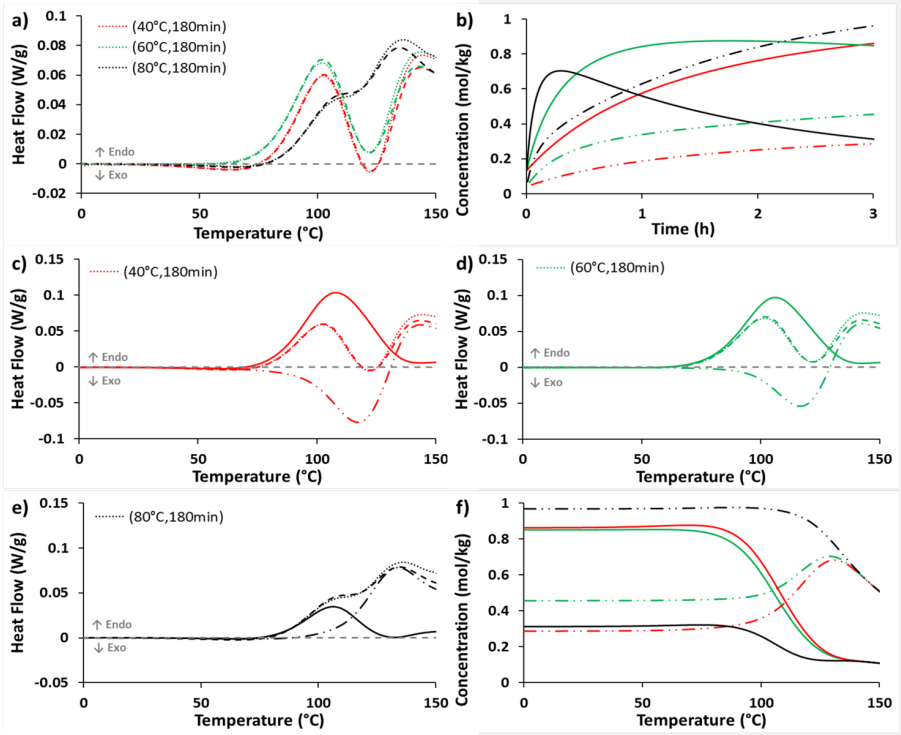

Figure 8: a) Overlay of the experimental (dotted line) and modelled (dashed line) heat flow profiles (exo down) for the heating after (40 °C,180 min), (60 °C,180 min) and (80 °C,180 min) for a F400-M400 (r=0.7) system. b) The concentration profiles of the endo (solid line) and exo adduct (dash double dot line) as a function of time during the isothermal segment. The heat flow due to the endo adduct (solid line) and exo adduct (dash double dot line) is overlayed with the experimental and modelled heat flow for c) (40 °C,180 min), d) (60 °C,180 min) and e) (80 °C,180 min). f) gives the corresponding concentration of the endo adduct (solid line) and exo adduct (dash double dot line) during the second heating.

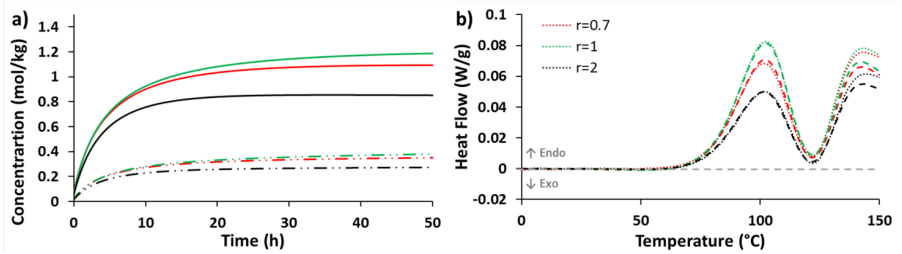

Figure 9: a) The concentration of the endo adduct (solid line) and exo adduct (dash double dot line) corresponding to microcalorimetry experiments for a F400-M400 system with r = 0.7, 1 and 2 at T_{iso}=25 °C. c) Overlay of the experimental (dotted line) and modelled (dashed line) heat flow profiles (exo down) for a heating after (60°C,180min) for r = 0.7, 1 and 2.

the start of the experiment, meaning that the Diels-Alder reaction proceeds the fastest at the start of the reaction. The higher the isothermal temperature, the higher the heat flow, and thus the faster the kinetics. Figure 6b shows the corresponding calculated concentration of the adducts as a function of time. Both adducts are initially formed faster at higher temperature, however, the rate difference between them becomes smaller. This can be observed from the values in Table 3 and in Figure 7a, where the higher the temperature (the lower the reciprocal temperature), the closer the logarithm of the forward rate constants are to each other. It is worth noting that the exo adduct does not become kinetically
favoured at relevant temperatures. Figure 7b shows no cross-over between the equilibrium constants of the endo and exo adducts, with the exo one being the higher one at all temperatures, proving once again that the exo adduct is thermodynamically the most stable at all temperatures.

Figure 8a shows the influence of the isothermal temperature (T_{iso}: 40 °C, 60 °C, and 80 °C) for the same isothermal time (180 min) at maleimide/furan ratio r = 0.7 on the heat flow profile from the second heating. The measurements with T_{iso} equal to 40 °C and 60 °C show two distinct endothermic peaks, for the cycloreversion of the endo and exo adducts, as can be seen from Figure 8c and 8d. However, in both cases an exothermic contribution is seen in the heat flow profile of the exo adduct, since the furan and maleimide formed during the cycloreversion of the endo isomer are (partially) being consumed to form additional exo adduct (Figure 8f). During the isothermal segment (Figure 8b) it can be observed that both at 40 °C and 60 °C the endo adduct is formed predominantly after 180 min. For the measurement at 80°C, the endo adduct prevails at the start of the isothermal section, however, within the 3 h reaction time the ratio has shifted in favour of the exo adduct, the crossover of the adduct concentrations already happens after 1 h (compared to 9 h at 60 °C, Figure 4). This explains why for the reaction heat flow trace of 80 °C in Figure 8a the cycloreversion of the endo adduct only shows as a shoulder to the much bigger cycloreversion of the more abundant exo adduct. In the heat flow profile for 80 °C (Figure 8e), no exothermic peak is seen corresponding to the formation of additional exo isomer, and in the concentration profile (Figure 8f) no increase in exo adduct is seen for 80 °C (in contrast to the results for 40 °C and 60 °C). The results clearly indicate that the temperature treatment and thermal processing conditions strongly influence the exo/endo isomer ratio in reversible polymer network systems based on the furan-maleimide Diels-Alder reaction.

Influence of the maleimide furan ratio

Isothermal (Figure 9a) and non-isothermal (Figure 9b) data for F400-M400 system with different stoichiometries show that the exo/endo ratio is not markedly influenced by the initial maleimide/furan ratio. The more off-stochiometric, the less endo and exo adduct is formed in isothermal conditions (Figure 9a) and the lower the measured heat flows in the heating after an isothermal treatment (Figure 9b). The exo/endo ratio is thus mainly influenced by temperature and the time stayed at that temperature.

Implications for applications

The reversible Diels-Alder reaction is becoming increasingly popular for the creation of thermoresponsive polymer networks [2,3]. Here, the effect of the stereochemistry on the dynamic character of the thermoreversible Diels-Alder reaction is discussed in view of advanced processing, self-healing applications and long-term stability. In previous paragraphs (Figures 4 and 5) it was shown that, at ambient temperature, the kinetically favoured endo isomer is formed

Table 4: Optimization of the reaction conditions and thermal stability: (left) isothermal reaction time to reach 95 % of the equilibrium conversion at the isothermal temperature and (right) the time to reach 95 % of the equilibrium conversion at 25 °C.

	95 % of $x_{tot\ eq.,T}$		95 % of $x_{tot\ eq.,25°C}$			
Temperature (°C)	**Time at T (h)**	**% of $x_{tot\ eq,25\ °C}$ (%)**	**Time at 25 °C (h)**	**Total time (h)**	**A_{endo} (mol/kg)**	**A_{exo} (mol/kg)**
120	0.10	56	55.5	55.6	0.66	0.94
110	0.22	63	53.5	53.8	0.62	0.99
100	0.51	69	50.8	51.3	0.57	1.03
90	1.2	75	47.6	48.8	0.54	1.07
80	3.0	80	44.0	47.0	0.52	1.08
70	7.8	84	39.5	47.2	0.53	1.08
60	20.6	88	34.2	54.9	0.56	1.04
50	51.5	91	29.0	80.5	0.67	0.93
25	87.7	95	0	87.7	1.20	0.40

faster and is gradually replaced by the thermodynamically more stable exo isomer over time. The maximum conversion that could be achieved if only one adduct were present, is higher for the thermodynamically more stable exo isomer ($x_{exo\ eq.,25°C}$ is 97 %) than for the endo isomer ($x_{endo\ eq.,\ 25°C}$ is 91 %). As a result, the total conversion increases as a function of time, illustrated in Figure 10 for isothermal reaction at 25 °C. The largest contribution to the total conversion (grey dash-dotted line) is due to the simultaneous formation of both adducts in the first stage of the reaction (~3 days). In a second stage, the biggest shift from the endo to the exo isomer is observed, with a clear crossover after about 50 days. The total conversion continues to rise for several hundreds of days, slowly approaching its 'final' level. The differences in conversion between 3 days and 3 years of reaction are listed in Table 5, showing an additional increase of 5 % conversion. For practical applications of these materials, it is important to have good control over the Diels-Alder conversion, since the conversion determines the crosslink density, which in turn defines the glass transition temperature and the mechanical properties of the polymer network. The slow increase in conversion over time can be minimized by adjusting the processing conditions in such a way that a maximum amount of exo adduct is formed already during processing.

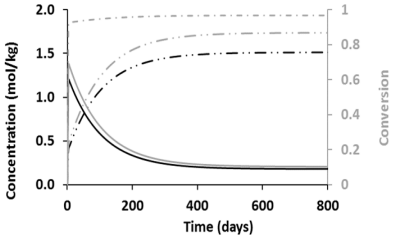

Figure 10: Evolution of the endo (solid line) and exo (dash double dot line) adduct concentration (black) and conversion (grey) for a F400-M400 (r=1) system at 25 °C. The total conversion is given by the grey dash dot line.

Table 5: The effect of stereochemistry on the long-term properties: conversion, glass transition and gel transition.

Parameters	**Endo-rich**	**Exo-rich**
Time @ 25 °C	3 days	3 years
% exo isomer	25 %	89 %
x	0.92	0.97
T_g	2.0	6.3
$T_{gel,\ eq}$	119 °C	
% exo isomer	84 %	
T_{gel} @ 1 °C min^{-1}	121 °C	121 °C
% exo isomer	85 %	85 %
T_{gel} @ 10 °C min^{-1}	113 °C	135 °C
% exo isomer	43 %	92 %
T_{gel} @ 100 °C min^{-1}	136 °C	158 °C
% exo isomer	39 %	97 %

Table 4 compares isothermal treatments at different temperatures followed by post-treating at 25 °C, and the effect on the total time required to achieve at 25 °C 95 % of the total equilibrium conversion at 25 °C, $x_{tot\ eq.,25\ °C}$, as well as the concentrations of endo and exo adduct formed at that stage. The treatment of 3 h at 80 °C results in a conversion that is already 80 % of $x_{tot\ eq.,25\ °C}$ and results in the minimum total time (47 h) to reach 95 % of $x_{tot\ eq.,25\ °C}$ and the largest concentration of exo adduct. This can be compared with the 88 h needed when reacting at 25 °C and an exo adduct concentration that has almost tripled. This demonstrates that using a dedicated thermal treatment, materials with more stable properties are obtained. Note that the optimal temperature programme depends on the reactivity and concentrations of the functional groups. A further increase of the conversion results in an increase of the glass transition temperature T_g of the polymer network. The T_g-x relationship is given by the DiBenedetto model (equation 9).

Table 6: Optimized values of $T_{g\,x=0}$, $T_{g\,x=1}$ and λ for F400-M400 when considering only one isomer or both isomers.

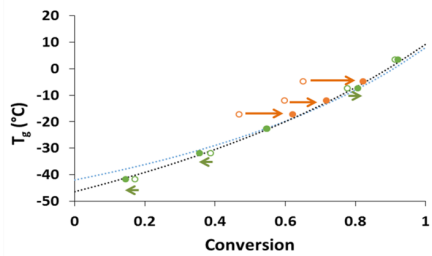

Figure 11: *Tg-x* relationship for a F400-M400 (*r*=1) system with conversions calculated for a single equilibrium based on kinetic parameters from [20] (blue dotted line and empty circles) compared to the model taking into account both stereoisomers (black dotted line and solid circles) with exo/endo ratio smaller than 1 (green) and larger than 1 (orange).

Parameters	One isomer[20]	Two isomers
$T_{g\,x=0}$	-42	-46
$T_{g\,x=1}$	8	9
λ	0.53	0.60

Figure 11 shows the experimental (circles) and modelled T_g (dotted lines) as a function of the simulated conversion, based on the thermal history of the material. It should be noted that the kinetic model is only reliable in situations without vitrification, as diffusion limitations on the reaction kinetics are not accounted for. This condition is satisfied for the experiments used as the curing temperature is always well above the end of the glass transition. Accounting for the formation of both endo and exo adducts, a nicely fitting T_g-*x* relation and an optimized lambda of 0.60 are obtained (Table 6), which is in good agreement with the expected value of 0.64 as the ratio between $\Delta C_{P\,x=1}$ and $\Delta C_{P\,x=0}$ [24–26]. Using this relationship, the T_g of a sample with 75 % endo adduct and a conversion of 92 % equals 2.0 °C (Table 5). The T_g increases by 4.3 °C as the conversion becomes 97 % after about 3 years at 25 °C. Figure 11 also shows the T_g-*x* relationship previously determined for the same material taking into account the formation of only one adduct (blue dotted line).[20] For materials with a high endo isomer content (green bullets) the one-equilibrium and two-equilibrium models correspond well, since the measurements conducted to set up the original T_g-*x* relationship were performed in experimental conditions where predominantly endo isomer is formed, and that the single equilibrium kinetic data correspond fairly well to the kinetic data found for the endo adduct (Table 2). For materials with a high exo isomer content (orange bullets) the differences in conversions calculated are much larger. The one-equilibrium model strongly underestimates the conversion reached.

$$\frac{T_g - T_{g\,x=0}}{T_{g\,x=1} - T_{g\,x=0}} = \frac{\lambda x}{1 - (1-\lambda)x} \quad (9)$$

Furthermore, as the exo isomer is thermodynamically more stable than the endo adduct the reversible gel transition

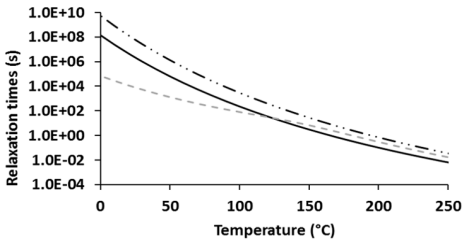

Figure 12: The relaxation time constant τ_{DA} of the double equilibrium (dashed grey line) (equation 11) and the lifetime of the cycloadduct τ_{rDA} (black)(equation 10) for the endo (solid line) and exo (dash double dot line) adduct.

temperature will be higher for materials with a higher exo isomer content. The gel transition temperature is the temperature at which the material behaviour changes from predominantly elastic to viscous behaviour. This gel transition occurs at a conversion that is fixed by the functionality of the monomers. The gel conversion for a 4 + 2 system is 0.577, according to the Flory-Stockmayer gel criterium. The temperature and time at which this gel transition occurs depend on the heating rate, as the temperature program determines the conversion of the system. Table 5 (figures in supplementary information) compares the gel transition temperatures for materials with a high endo content and a high exo content at different heating rates. At a heating rate of 1 °C min^{-1} both materials with low and high exo isomer content are close to equilibrium at high temperatures, resulting in similar T_{gel} close to the equilibrium gel transition temperature $T_{gel,eq}$ of 120 °C. At a heating rate of 10 °C min^{-1} the endo-rich material does not get the time to go to equilibrium and the endo isomers dissociate at a lower temperature, resulting in a T_{gel} lower than $T_{gel,eq}$. Heating up faster at 100 °C min^{-1} does not give enough time for the reaction kinetics to break the adduct bonds and a T_{gel} higher than $T_{gel,eq}$ is expected. For the exo-rich material the T_{gel} is always higher than that of the endo-rich material with increasing heating rate. This implies that higher temperatures and/or longer times will be required for reprocessing of exo-rich reversible networks.

The responsiveness of the dynamically reversible Diels-Alder polymer networks depends on two important time constants[27]. The first time constant is the lifetime of the cycloadduct τ_{rDA}, shown in Figure 12 by the black lines and given by Equation 10 for each stereoisomer. As temperature increases, τ_{rDA} decreases, and hence, the dynamic character of the reversible reaction increases and heating-mediated healing will proceed faster. The cycloadduct lifetime is also important for stress relaxation and creep in the dynamic covalent network, as the stress relaxation time for a reversibly associating network is proportional to the cycloadduct lifetime[28]. It should be noted that each cycloadduct isomer has its own lifetime, and hence, different stress relaxation behaviour. However, the cycloadduct lifetime of the endo isomer will dominate stress relaxation, as it is at least one order of magnitude smaller than that of the exo adduct in the considered temperature range. The second time constant is the relaxation time of the chemical equilibrium τ_{DA}, defining the time it takes to return to equilibrium at a certain temperature after the equilibrium was perturbed. The relaxation time for the parallel and dependent formation of the two stereoisomers is given by Equation 11 (see supplementary information for derivation) and shown in Figure 12 by the grey line. In the case of autonomous healing upon mechanical activation, without additional heating, the relaxation time τ_{DA} determines the time necessary to reform a fraction of the broken bonds. Both endo and exo cycloadduct bonds will be broken to form free furan and maleimide groups and both stereoisomers will be formed again to restore the equilibrium state. One can expect that the kinetically favoured endo adduct will be formed predominantly in the first stage of the restoration of the equilibrium as also seen for isothermal reactions at low temperatures. The freshly formed endo adduct than transforms into the more stable exo adduct again on a different timescale. Moreover, for a material with a high exo isomer content a slower response to a thermal perturbation is expected, for example for heating-mediated healing, similarly to thermal processing.

Conclusions

The influence of the stereochemistry of the Diels-Alder reaction between a furan and maleimide group on the reaction kinetics was studied in the absence of a solvent using calorimetry. Using a mechanistic model involving the Diels-Alder and retro-Diels-Alder reactions for each cycloadduct, isothermal and non-isothermal calorimetric experimental data were modelled. The influence of well-designed isothermal treatments (time and temperature) and the maleimide/furan stoichiometric ratio on the ratio of the concentrations of exo and endo isomer were studied to further improve the reliability of the kinetic model parameters. The success of the model corroborates that the isomerization from the endo to exo adduct is preceded by the cycloreversion of the endo adduct into its monomers, as previously stated in literature. The reliability of the obtained model was confirmed by a successful comparison between the model and experimental data for the furan, maleimide, endo adduct, and exo adduct concentrations obtained using time-resolved liquid state ^{1}H NMR spectroscopy for an isothermal reaction.

The obtained kinetic and thermodynamic parameters confirmed that the endo adduct is kinetically the fastest, while the exo adduct is thermodynamically more stable over the entire temperature range. For isothermal reactions, this results in a crossover between the exo and endo adduct concentration and an increase in exo/endo isomer ratio over time. At elevated temperatures this crossover occurs within hours, whereas at ambient temperature it takes over 50 days. This change in exo/endo ratio influences the final conversion and consequently the crosslink density, the glass transition temperature and the mechanical properties of the polymer network even after processing over long periods of time. This chemical ageing effect could be minimized by optimizing the processing conditions to purposely create a high exo adduct content in the produced materials to improve the stability of the conversion and the material properties. This is important in applications where the mechanical properties of the material determine the performance of a structure or a machine, such as in robotic actuators.

The calorimetric approach used in this work for studying the kinetics of the two stereochemical isomers could be used for studying the reaction kinetics for modified furans, aiming at the tuning of the thermoreversible reactions for different applications, such as self-healing and stimuli-responsive adaptable networks, and are generally applicable to the study of other (condensed-state) cycloaddition reactions.

$$\tau_{\mathrm{rDA}} = \frac{1}{k_{\mathrm{rDA}}} \tag{10}$$

$$\tau_{\mathrm{DA}} = \frac{1}{\left(k_{\mathrm{DA,endo}} + k_{\mathrm{DA,exo}}\right)\left([\mathrm{F}]_e + [\mathrm{M}]_e\right) + \mathrm{a}} \tag{11}$$

$$\text{with } a = \frac{k_{rDA,\mathrm{endo}} K_{\mathrm{endo}} + k_{rDA,\mathrm{exo}} K_{\mathrm{exo}}}{K_{\mathrm{endo}} + K_{\mathrm{exo}}}$$

Conflicts of interest

There are no conflicts to declare.

Acknowledgments

The authors would like to acknowledge Hartmut Fischer for the fruitful discussion that lead to this study. Luk Van Lokeren and Ingrid Verbruggen are appreciated for their help with the NMR measurements. The Research Foundation of Flanders (FWO) is acknowledged for the PhD fellowship of Audrey Cuvellier (1S40617N) and Robrecht Verhelle (1S69116N). This work was partially funded by the European Commission ERC starting grant SPEAR (no. 337596).

Notes and references

1 O. Diels and K. Alder, *Leibigs Ann. Chem.*, 1928, **460**, 98–122.
2 X. Chen, M. A. Dam, K. Ono, A. Mal, H. Shen, S. R. Nutt, K. Sheran and F. Wudl, *Science (80-.).*, 2002, **295**, 1698–1702.
3 M. Wouters, E. Craenmehr, K. Tempelaars, H. Fischer, N. Stroeks and J. Van Zanten, *Prog. Org. coatings*, 2009, **64**, 156–162.
4 G. Scheltjens, J. Brancart, I. De Graeve, B. Van Mele, H. Terryn and G. Van Assche, *J. Therm. Anal. Calorim.*, 2011, **105**, 805–809.
5 J. Brancart, G. Scheltjens, T. Muselle, B. Van Mele, H. Terryn and G. Van Assche, *J. Intell. Mater. Syst. Struct.*, 2014, **25**, 40–46.
6 G. Scheltjens, M. M. Diaz, J. Brancart, G. Van Assche and B. Van Mele, *React. Funct. Polym.*, 2013, **73**, 413–420.
7 S. Terryn, G. Mathijssen, J. Brancart, D. Lefeber, G. Van Assche and B. Vanderborght, *Bioinspiration and Biomimetics*, 2015, **10**.
8 S. Terryn, J. Brancart, D. Lefeber, G. Van Assche and B. Vanderborght, *IEEE Robot. Autom. Lett.*, 2017, **3**, 16–21.
9 S. Terryn, J. Brancart, D. Lefeber, G. Van Assche and B. Vanderborght, *Sci. Robot.*, 2017, **2**, 1–12.
10 F. Fringuelli and A. Taticchi, *The Diels-Alder reaction*, Wiley and sons, 2002.
11 J. G. Martin and R. K. Hill, *Chem. Rev.*, 1961, **61**, 537–562.
12 M. W. Lee and W. C. Herndon, 1978, **43**, 518.
13 M. M. Diaz Acevedo, Vrije Universiteit Brussel, 2016.
14 Štirn, A. Ručigaj and M. Krajnc, *Express Polym. Lett.*, 2016, **10**, 537–547.
15 B. J. Adzima, H. A. Aguirre, C. J. Kloxin, T. F. Scott and C. N. Bowman, *Macromulecules*, 2008, 9112–9117.
16 L. Rulisek, P. Sebek, Z. Havlas, R. Hrabal, P. Capek and A. Svatos, *J. Org. Chem.*, 2005, **17**, 6295–6302.
17 A. Buonerba, R. Lapenta, S. Ortega Sánchez, C. Capacchione, S. Milione and A. Grassi, *ChemistrySelect*, 2017, **2**, 1605–1612.
18 B. Froidevaux, V. , Borne, M. , Laborbe, E. , Auvergne, R. , Gandini, A. , Boutevin, *RSC Adv.*, 2015, **5**, 37742–37754.
19 M. A. Amman C, Meier P, *J. Magn. Reson.*, 1982, **46**, 319–321.
20 M. M. Diaz, G. Van Assche, F. H. J. Maurer and B. Van Mele, *Polym. (United Kingdom)*, 2017, **120**, 176–188.
21 K. J. Jones, I. Kinshott, M. Reading, A. A. Lacey, C. Nikolopoulos and H. M. Pollock, *Thermochim. Acta*, 1997, **305**, 187–199.
22 B. D. Mather, K. Viswanathan, K. M. Miller and T. E. Long, *Prog. Polym. Sci.*, 2006, **31**, 487–531.
23 J. Canadell, H. Fischer, G. De With and R. A. T. M. Van Benthem, *J. Polym. Sci. Part A Polym. Chem.*, 2010, **48**, 3456–3467.
24 A. T. DiBenedetto, *J. Polym. Sci. Part B Polym. Phys.*, 1987, **25**, 1949–1969.
25 P. R. Couchman, *Macromolecules*, 1987, **20**, 1712–1717.
26 J. P. Pascault and R. J. J. Williams, *J. Polym. Sci. Part B Polym. Phys.*, 1990, **28**, 85–95.
27 M. M. Diaz, J. Brancart, G. Van Assche and B. Van Mele, *Polymer (Guildf).*
28 M. Rubinstein and A. N. Semenov, 1998, **31**, 1386–1397.